Flight Test Results for Autonomous Icing Protection Solution for Small Unmanned Aircraft

Kim Lynge Sørensen*, Tor Arne Johansen*
*Department of Engineering Cybernetics, Centre for Autonomous Marine Operations and Systems,
The Norwegian University of Science and Technology. kim.sorensen@ntnu.no, and tor.arne.johansen@ntnu.no

***Abstract*—The primary focus of the work presented in this paper is a proof-of-concept study of a novel electro-thermal-based autonomous icing protection solution (IPS) for small unmanned aircraft. The solution includes a central control unit, where several control algorithms, ensure temperature control of electro-thermal sources, applied to exposed aircraft surfaces. The solution includes three different control procedures (icing detection, anti-icing, and de-icing) that are validated through test flights conducted in Ny-Ålesund, Svalbard, Norway.**

***Keywords*—Unmanned Aircraft, UAVs, Aircraft Icing, Electro-Thermal Icing Protection;**

I. Introduction

The use of unmanned aerial vehicles (UAVs) has increased significantly over the last decade, operating in surveillance and reconnaissance, search and rescue, telecommunications, scientific data acquisition, inspection, etc. UAVs are very well suited for operating in conditions that are deemed hazardous or unsafe for human pilots, such as the Arctic and Antarctic. Consequently, reliable and efficient UAV operations, regardless of atmospheric conditions, are a necessity.

In aviation, icing conditions are atmospheric conditions that can lead to the formation of ice on exposed aircraft surfaces. In-flight icing can occur when an aircraft passes through air that contain droplets of water (humid air), and where the temperature at the point of the droplets impact with the aircraft, is 0°C or colder. The effects of icing depends upon the location, and the type of the formed ice. Icing can occur on wings, propellers, control surfaces, horizontal and vertical stabilizers, fuselage nose, landing gear doors, engine intakes, fuselage air data ports and sensors, and drain system outputs [6, 7, 11]. Concerning the work presented in this paper, emphasis has been put on leading edge wing icing.

For conventional aircraft a wide variety of IPS are commercially available. These can be classified into three different categories depending on their common usage. The categories are 1) thermal-based methods, 2) mechanical based methods, and 3) chemical-based methods.

In the thermal-based category the most common systems are hot air and electro-thermal. The hot air systems typically rely on the high temperature bleed-air from the engine compressor gas or hot exhaust gas, which is transferred to relevant icing exposed surfaces by piccolo tubes. Electro-thermal systems include thermal sources, usually electric heating blankets embedded in the wing structure, under the skin-surface on - and around - the leading edges of the wings and stabilisers. Recently developed conductive polymer nano-composites could eventually render the use of heating blankets moot, however, these composites will not change the fundamental concept behind thermal-based icing protection systems.

The category of mechanical-based icing protection systems could be denominated surface deformation systems. This category of systems can be divided into three sub-categories labelled, 1) pneumatic boots, 2) electromagnetic impulse de-icing, and 3) electromagnetic expulsive boots. The systems labelled pneumatic boots are the most commonly applied systems, employing surface deformation, on conventional aircraft. Pneumatic boots are essentially a thick inflatable rubber membrane bonded to surfaces that require icing protection. When ice has accreted on the rubber membrane it is inflated, imposing bending and shear stresses on the ice layer, which in turn breaks the ice into small pieces that are carried downstream by aerodynamic forces. The two remaining sub-category systems are based on the same principle as the pneumatic boots, although they employ electromagnetic impulses to shed icing.

Chemical-based icing protection can be divided into two sub-categories, 1) ground and 2) in-flight. The prior indicate the icing solution, where certain chemicals (typically ethylene glycol) are applied to exposed aircraft surfaces, thereby lowering the freezing temperature of liquid water. The latter sub-category is generally denoted the weeping wing solution, as chemicals are exuded in-flight through nozzles in the leading edge of the wings and stabilisers. [2, 14, 15, 18].

Note that autonomous icing detection and mitigation is not included in conventional aircraft icing protection systems. The reason for this absence is that icing detection is accomplished by the pilots visual confirmation, or through sensors (typically optical) that alert the pilot. Once icing has been established the pilot manually activates any icing protection deemed necessary.

As technology has advanced, improved methods of ice detection have been developed. Presently various icing detector sensors are commercially available. These, however, are typically highly expensive in a small UAV context.

Another icing detection approach is through algorithms using avionics and indirect sensor measurements. The review of icing detection approaches presented in [3] includes a comparison between existing methods; observer-based algorithms, batch least-squares algorithms, neural networks based algorithms, H_∞ based algorithms, and a combination of neural networks and *Kalman* filtering techniques. The study reveals that among the mentioned approaches, it is the H_∞ and the neural networks combined with Kalman filtering techniques that provide timely and more accurate icing indication. In [24] and [25] icing is diagnosed through an observer-based fault

diagnosis technique that detects and estimates the percentage of ice present on the aircraft wing, relying on a linearised lateral model of the aircraft. In [4] the icing detection problem is cast in a multiple-model framework and based on a linearised longitudinal model of the aircraft. A bank of possible system models, whose structure is based on Krener min-max observers, is defined, each one corresponding to a different claimed value of the icing severity factor. Overall state and icing factor estimates are obtained as weighted combinations of the states of the models and the claimed icing values, respectively. In [16] icing detection is addressed using a linear parameter varying (LPV) unknown input observer based approach. A decision algorithm identifies unexpected system dynamics caused by icing through the analysis of temporal and low-frequency residuals. The proposed approach is validated through a case study. Further, this work has been extended in [17], where an LPV proportional integral unknown input observer is used to diagnose actuator faults and icing for UAVs. This approach is more robust towards noise and also includes a wind to noise ratio allowing for optimal tuning of relevant design parameters. The approach is validated through simulations. The work described in [5] applies an approach similar to the one presented in [16], but for over-actuated UAVs. In [1] in-flight parameter estimation of dynamic aircraft parameters is completed, using a *Hinf* parameter identification algorithm. Subsequently, icing detection and location is provided by the application of a probabilistic neural network (supplied with a database corresponding to various icing locations and severities for training purposes), receiving the parameter estimates as inputs. A simulation study of the approach reveals promising results. The work presented in [9] has a different approach altogether. Here aligned Carbon nanotubes (CNTs) are applied as a separate surface layer. This layer is then heated through electrical heating. A change in heat capacity will then signify an additional material, such as water or ice. This approach assume that certain parameters have a constant behaviour and that the additional material has significant mass.

A recurring subject in icing protection solutions is icephobic external surface materials that in essence should repel the ice and minimise ice adhesion. With the advent of nanotechnology, the spectra of potential materials that may fulfil the desired characteristics related to low ice adhesion have expanded considerably. So far, solutions of this type have challenges to overcome before they could be considered a viable alternative to conventional systems. To mention a few; the material has to withstand erosion, stress, and other weathering conditions in terms of its structural integrity. The material needs to preserve its initial characteristics related to icephobicity regardless of erosion and corrosion [8]. Finally, the material should be inexpensive to manufacture, easy to apply, and environmentally friendly.

The autonomous IPS presented in this paper is fundamentally different than typical commercial IPS' found in the literature and industry today, as full autonomy is the fundamental design criterion.

The remainder of the paper is organized as follows. In Section II, an architectural overview of the autonomous icing protection solution (IPS) for small UAVs is presented. Section III provides a proof-of-concept study for various applications of the IPS and the paper is concluded with section IV.

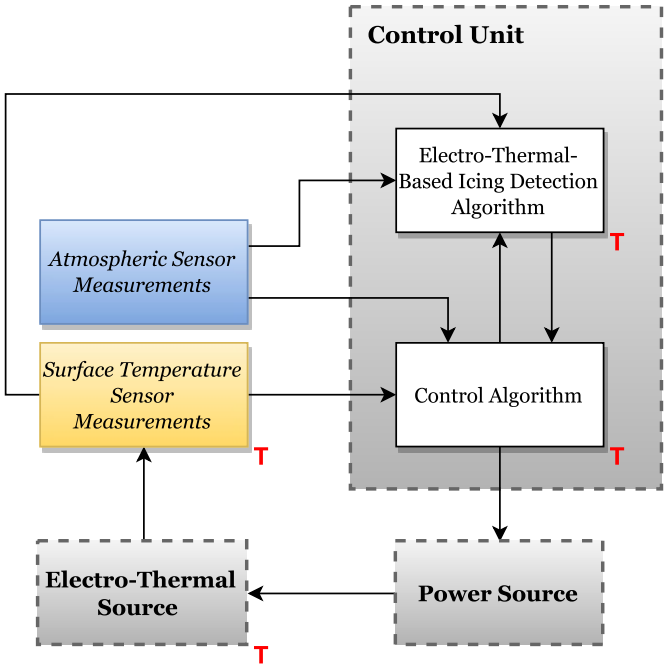

Fig. 1: Icing protection solution - architectural overview.

II. Icing Protection Solution

Aircraft IPS typically include means of detecting icing and an active de-ice or anti-ice element. Generally de-icing entails a removal of accreted ice, while anti-icing signifies an altogether prevention of icing. For conventional aircraft such systems have been a part of design solutions for decades. However, for the relatively young developing industry of unmanned aircraft, particularly for small UAVs, no commercially available solution exists. Icing protection systems (or solutions) for small unmanned aircraft is a new field of research, as such UAV specific literature on this subject is only sparsely represented. Note that icing protection solutions for conventional aircraft are generally not suitable for smaller UAVs as they are either structurally invasive, expensive, heavy, or environmentally harmful. Common for all of these solutions is the requirement of human interaction.

A. Autonomous Icing Protection Solution - Unmanned Aircraft

Here we consider an IPS that comprise three primary elements, 1) electro-thermal sources, applied to exposed aircraft surfaces, 2) a central control unit, and 3) an energy source. The control unit is primed by an on-board atmospheric sensor package, measuring ambient atmospheric conditions. Once the risk of icing is established, ice detection algorithms are activated. If ice is detected, control algorithms controls the energy supplied to the electro-thermal sources, thereby achieving temperature control of said sources. The overall functionality of the proposed IPS, running in a de-icing mode, is illustrated by the high level state diagram found in Figure 2.

The solution is composed of several components as seen in Figure 1. The following is an overview of parts of an icing

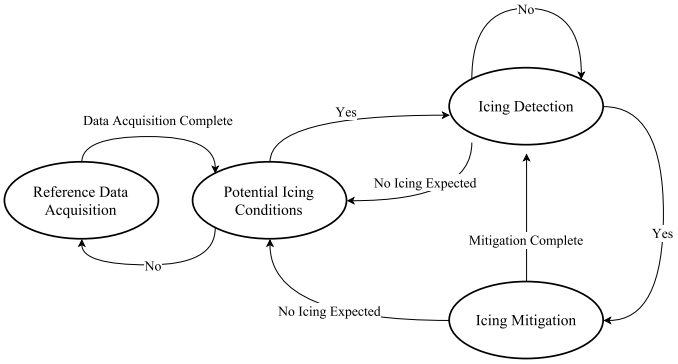

Fig. 2: Icing protection solution (de-icing mode) - state diagram.

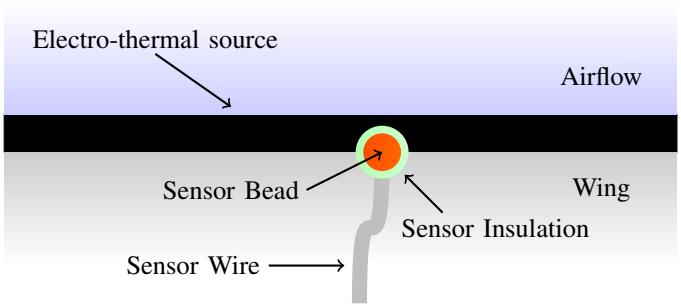

Fig. 3: Temperature sensor embedded in wing and electro-thermal source.

protection solution developed by the authors, and is based on the work found in [21, 22]

Regarding Figure 1 and the overall architecture of the solution, it should be noted that there is *one* atmospheric sensor package and *one* power source, for the aircraft in its entirety. All the other components (internal and external to the control unit) have duplicates. These duplicates indicate that each wing has an electro-thermal source and therefore require individual feedback and algorithms for detection and control.

As seen in Figure 1, sensor measurement blocks provide measurements to the control unit. A brief explanation follows and a diagram of the IPS (of the physical layout), integrated onto an X8 Skywalker UAV platform (the testbed UAV platform applied for the work presented in this paper), is found in Figure 4.

- The atmospheric sensor provides both ambient temperature- and relative humidity measurements.
- The surface temperature sensor measurements is comprised of sensors (one or more) embedded in each wing underneath an electro-thermal source. These sensors supply the control unit with temperature measurements of the electro-thermal sources.

Note that the temperature distribution over the leading edge of wings is non-uniform, hence embedding more sensors enables for a more accurate representation of the temperature distribution in the electro-thermal source. Another benefit of multiple sensors is that of redundancies in the event of sensor failure, where fault diagnosis would further enhance robustness of the proposed solution.

Electrically insulating the embedded temperature sensors from the electro-thermal source is necessary, as the high levels of electric current running through an activated electro-thermal source will disrupt sensor measurements. Further, due to the size of the temperature sensor, the sensor bead is partly embedded in the electro-thermal source and the wing as illustrated in Figure 3.

Two of the primary elements of the solution presented in this paper are the electro-thermal sources and the power source, both found in Figure 1.

- The composition of the electro thermal sources is based on Carbon Nano materials and is applied through a liquid carrier (a coating). The internal resistivity of the electro-thermal source is based on the thickness of any applied layer, area-size of said layer, and concentration of the carbon nanomaterial in the coating.
- The power source can either be a battery pack, typically lithium polymer batteries, or power can be supplied by the aircraft engine through a generator.

Power is supplied to the electro-thermal source through a copper bus-bar located on the wings of the aircraft, as seen in Figure 4a. Here it should be noted that the thickness, location, and layout of the electro-thermal source is directly linked to power consumption. Optimizing these three aspects is key to achieving the highest level of performance.

The last of the primary elements that constitute the solution presented here is the central control unit, whose components and function will be presented in the following.

B. Central Control Unit

The central control unit depends on external inputs processed by internal components. As seen in Figure 1 these components combined with the external inputs form a system of interconnections ultimately enable the icing protection solution to perform in complete autonomy. The following will take this system apart, describe each component in more detail, and explain how each contributes to the performance and reliability of the combined solution.

The Electro-Thermal-Based Icing Detection Algorithm (ETB-IDA) addresses the issue of icing detection in a fault diagnosis framework and applies a model of the thermodynamic system surrounding the aircraft wings and the electro-thermal source. The model of said system includes the composite structure of the wing and the electro-thermal source, the airflow around the wing, water layers, and an ice layer. The thermodynamic phenomena concerned with aircraft icing, with no external sources, can be cast in an energy balance framework as

$$\dot{q}_C + \dot{q}_d + \dot{q}_e + \dot{q}_s + \dot{q}_r = \dot{q}_a + \dot{q}_k + \dot{q}_l, \qquad (1)$$

with a representation of the components supplied in Table I.

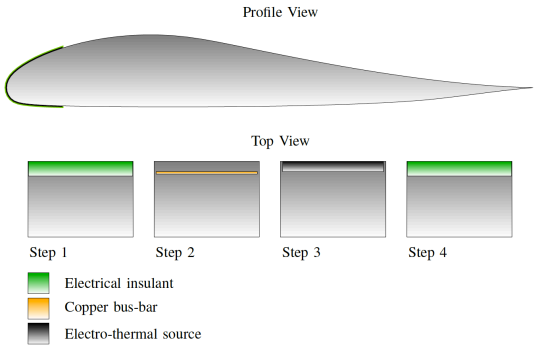

(a) Application procedure of electro-thermal source to leading edge of aircraft wing

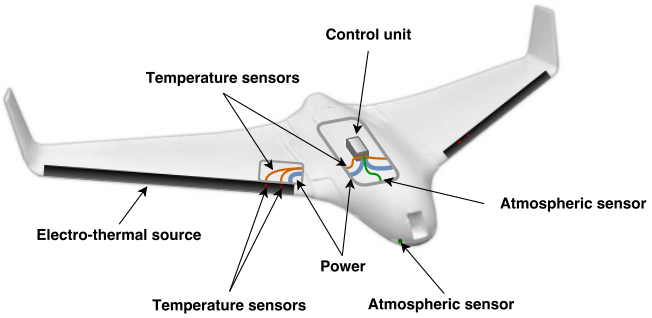

(b) Integrated IPS onto X8 Skywalker UAV platform.

Fig. 4: Electro-thermal source application steps and physical layout of IPS on X8 Skywalker UAV platform.

Symbol	Description
$\dot{q}_C$	Convective heat transfer
$\dot{q}_c$	Conductive heat transfer
$\dot{q}_d$	Cooling by incoming liquid water droplets
$\dot{q}_e$	Evaporative heat loss
$\dot{q}_s$	Sublimative heat loss
$\dot{q}_r$	Radiative heat loss
$\dot{q}_a$	Aerodynamic heating
$\dot{q}_k$	Kinetic energy from incoming liquid water droplets
$\dot{q}_l$	Latent heat of solidification

TABLE I: Thermodynamic phenomena.

Introducing an external heat source ($\dot{q}_{ext}$) into (1) the heat rate of a thermodynamic system ($\dot{q}_{sys}$) surrounding a given aircraft surface area (flying in icing conditions) can be expressed by

$$\dot{q}_{sys} = -\dot{q}_C - \dot{q}_c - \dot{q}_d - \dot{q}_e - \dot{q}_s - \dot{q}_r + \dot{q}_a + \dot{q}_k + \dot{q}_l + \dot{q}_{ext}. \quad (2)$$

For such a system the rate of thermal dissipation can be equated with the decrease in temperature of the body volume (the volume of the external heat source) over time as

$$\rho c_p V \frac{dT_s}{dt} = -\dot{q}_C - \dot{q}_c - \dot{q}_d - \dot{q}_e - \dot{q}_s - \dot{q}_r + \dot{q}_a + \dot{q}_k + \dot{q}_l + \dot{q}_{ext}, \quad (3)$$

where ρ, c_p, and V denote the density, specific heat capacity, and volume of the external heat source, respectively. T_s is the point temperature of the relevant outer surface.

To explore the dynamics of (3) in an icing detection perspective several simplifying assumptions are imposed.

- Thermal conduction ($\dot{q}_c$) in this context implies heat flowing from the electro-thermal source to the wing structure. In the framework applied here thermal convection and conduction are initially proportional to the same temperature difference ΔT, with different proportionality coefficients k and h, for conduction and convection respectively. The reason for discarding conduction of this type in the subsequent presentation relates to the ratio h/k, where $k << h$ [13]. Consequently the contribution from thermal conduction will be negligible compared to the contribution from thermal convection.
- Sublimation, evaporation, and latent heat of solidification ($\dot{q}_s$, $\dot{q}_e$, and $\dot{q}_l$, respectively) are discarded due to the limited phase change expected to occur during electro-thermal source temperature increases used to obtain the required data for the icing detection.
- Thermal dissipation by incoming liquid water droplets ($\dot{q}_d$) and the heat released through kinetic energy ($\dot{q}_k$) are not included in the subsequent considerations due to low airspeed and the transient response of the system.
- Thermal gain by aerodynamic heating ($\dot{q}_a$) is discarded as the surface of the aircraft are relatively smooth and the cruise airspeed is low.

It should be noted that the assumptions presented here greatly simplifies the thermodynamic system and is valid for steady flight with an approximately constant cruise airspeed and operational altitude. The simplifying assumptions just presented enable for the ordinary differential equation of (3) to be cast in a form ([20])

$$\frac{dT_s}{dt} + \frac{1}{\tau} T_s = \frac{1}{\tau} T_\infty, \quad (4)$$

dependent on a parameter (τ) denoted the thermal time constant, which is defined as

$$\tau \equiv \frac{\rho c_p V}{Ah}, \quad (5)$$

where A is the surface area and h is the convective heat transfer coefficient. T_∞ from (4) is the temperature of the ambient airflow. Note that for (4) and subsequent expressions $\dot{q}_{ext} = 0$.

Equation (4) suggests that the difference between the external heat source and the surroundings, as a function of time, can be represented by

$$\Delta T_s(t) = \Delta T_{s,0} e^{-\tau/t}, \quad (6)$$

where $\Delta T_{s,0}$ is the temperature difference $T_s - T_\infty$ at time $t = 0$. Equation (6) is the mathematical interpretation of the intuitive notion that the external heat source, once deactivated, assumes the temperature of the surrounding airflow at an exponentially decaying rate governed by the thermal time constant τ.

For detection purposes the expression on the right hand side of equation (6), including the theoretical thermal time constant of equation (5) serves as a reference. The left hand side of equation (6) is the measurable quantity. Consequently the residual can be defined as

$$r \equiv \Delta T_{s,0} e^{\tau/t} - \Delta T_s(t) \tag{7}$$

where r ≈ 0 when there is no ice and r $\neq 0$ when there is. For robust detection r is monitored over a time window and a threshold is employed to detect unexpected changes.

The underlying principle of the ETB-IDA is that the thermal time constant τ is influenced by the isolating effects of an icing layer on the electro-thermal source, as heat is dissipated through this layer of ice instead of directly into the incoming airflow. It is this change, from dissipation into an incoming airflow to dissipation into ice that serve as the conceptual foundation of the EBT-IDA.

The ETB-IDA introduced here operates in a form of symbiotic relationship with a specific control algorithm, as the ETB-IDA requires this control algorithm to operate a given control pattern, conversely the control algorithm requires knowledge about any icing instances on the wings. The mentioned control pattern allows for rapid and brief temperature increases of the electro-thermal source, enabling the detection algorithm to obtain estimates of wing surface temperature gradients (one for each wing). For reference these gradients are estimated under nominal flight conditions. If the temperature gradients differ from the ones obtained as a reference, potential icing is detected and the algorithm produces a signal that alerts the subsequent control algorithm component to the risk of icing.

Input from the control algorithm is required to determine active electro-thermal source periods. Input from the atmospheric sensor is needed to distinguish between reference data acquisition and data acquired for the purpose of icing detection. Further inputs are supplied by the surface temperature sensors embedded in each wing (and electro-thermal source).

The secondary objective of the control algorithms is to optimize power consumption, while mitigating or preventing ice occurrences on the leading edge of the aircraft wings. This objective is achieved through feedback control, of the electro-thermal sources, using the surface temperature sensor measurements that are continuously supplying redundant measurements of the electro-thermal source temperatures (i.e. surface temperature of the leading edge of each wing of the aircraft). When temperature control is required, the control algorithms generates signals to the power source commanding how much current should be supplied to the electro-thermal sources in a certain time period. As such the range of temperature control is tightly linked with the power source available, as well as the internal composition and structural layout of the electro-thermal sources.

The control algorithm is primed by the inputs from the atmospheric sensor component that indicate possible icing conditions through ambient temperature and relative humidity measurements. Potential icing conditions are considered present when the atmospheric sensor measurements indicates a relative humidity RH $\geq 50\%$ and ambient temperatures $T_\infty \leq 0°$C, parameter values that according to [10, 19, 23] are conducive to icing conditions.

The basis for the control algorithms required for the icing detection, de-icing, and anti-icing program routines is the proportional-integral-derivative (PID) controller, which can be expressed in the form

$$u(t) = K_p e(t) K_i \int_0^t e(\tau) d\tau + K_d \frac{de(t)}{dt}, \tag{8}$$

where K_p, K_i, and K_d, are all non-negative parameters (or gains) for the proportional, integral, and derivative term, respectively. $u(t)$ is the control output and $e(t)$ signify the error between the desired set-point for the controller and the electro-thermal source temperature.

The control algorithm has three primary procedures, icing detection, anti-icing, and de-icing. These entail different temperature setpoints and processes for switching the electro-thermal sources on and off.

- The objective of the icing detection procedure is to generate specific temperature profiles to be analysed by the ETB-IDA. This is achieved through actively using the electro-thermal sources in a heating pattern, where a short energy burst, supplied to the electro-thermal sources is followed by a longer period without.
- The anti-icing procedure is a preventive measure to in-flight aircraft icing. This procedure is tasked with ensuring that the temperature of the electro-thermal source is always at level, where icing cannot form on the protected surfaces. This can be achieved by maintaining a specific offset temperature above ambient, thereby inducing evaporation.
- The de-icing procedure mitigates ice occurrences, i.e. ice accretion to a certain extent is allowed, however, once icing is detected, this procedures requires rapid heating of the electro-thermal source (to shed icing occuerences), and a desired temperature in the range of $T_s \in [+10, +30]°$C [12].

III. Experiments

A proof-of-concept of concept study for the three control procedures have been conducted. The main contribution of this paper is the presentation of findings obtained from these flight tests conducted in Ny-Aalesund, Svalbard, Norway.

A. A Flying Icing Protection Solution

As one of the primary UAV platforms of the NTNU-UAV laboratory the X8 Skywalker has been subjected to numerous preliminary test flights. In late September 2015 the NTNU-UAV laboratory conducted operations together with the Northern Research Institute (NORUT) in Ny-Ålesund on Svalbard, Norway, and in mid-January 2016 the NTNU-UAV laboratory conducted operations at Udduvoll airfield, located outside Trondheim, Norway. The primary objective of these preliminary flight tests were to demonstrate the airworthiness of the solution when integrated onto the X8 Skywalker UAV platform, and to obtain data for various optimisation problems and safeguard investigations.

In April 2016 the X8 Skywalker - equipped with the IPS - was brought back to Ny-Ålesund, Svalbard, Norway, to

conduct multiple test flights. The objectives were to asses the icing-detection, de-icing and anti-icing program routines, and to obtain electro-thermal source temperature data from several sensors at various locations on the wing.

B. Test Flights Preliminaries

Three different tests were conducted, with multiple objectives. The three tests can be categorised as follows.

- *icing detection* – The objective of this test flight was twofold. One was the purpose of validating the icing detection data collection program routine. The other was to obtain data from multiple temperature sensors - located at various chord line lengths on the aerofoil - used to assess the non-uniformity of the temperature distribution during the activation icing detection program routine.
- *de-icing* – This test flight had the primary purpose of validating the de-icing program routine.
- *anti-icing* – The objective of this test flight was validation.

It should be noted that the X8 Skywalker platform was retro-fitted with an electro-thermal source on both wings. However, due to focus on power consumption and electro-thermal source temperature profiles it was deemed reasonable to use all available power on just one wing for proof-of-concept study. All flights were conducted in non-icing conditions, as such the decision to use only one electro-thermal source was not hazardous to operations.

For the purpose of assessing electro-thermal source temperature distribution in the longitudinal flight direction, temperature sensors were embedded at various chord line lengths on the aerofoil, as illustrated in Figure 5. This investigation was also the primary purpose of the layout of the electro-thermal source, which will be different in an optimal setting.

The sensor used for feedback control is denoted T_{ETS}, aside from this, sensors were embedded 'atop' approximately 40 mm from the leading edge of the aerofoil, one was located on the very leading edge, and finally a sensor was embedded 'under' approximately 20 mm from the leading edge of the aerofoil.

Peak power supplied to the electro-thermal source was approximately 450 W and average airspeed was 17 m/s.

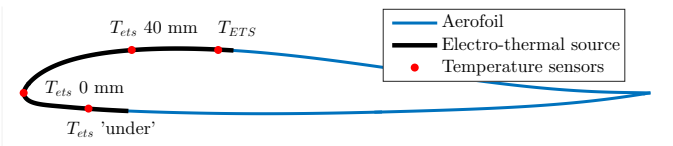

Fig. 5: Sensor locations on the X8 Skywalker wing used during the Svalbard April 2016 flight tests.

C. Test Flights - Results

The responses from the three test flights presented here can be found in Figures 6 – 8. All flights were conducted in non-icing conditions. The icing detection program routine was activated three times, at three different altitudes, during the icing detection test flight. Five temperature sensor responses were collected from sensors located as specified in Figure 5 and from the atmospheric sensor mounted on the main fuselage.

Note that the sample rates described in Figures 6 – 8 are incommensurable 2.6 Hz and 10 Hz for the *Arduino sample rate* and the *Neptus sample rate*, respectively.

The electro-thermal source temperature responses clearly display the expected and desired evolution of a rapid temperature increase, when the electro-thermal source is activated, and decrease, when it is de-activated. It's interesting to note the modest temperature increase of the sensor located at the very leading edge (T_{ets} 0 mm), even though approximately 450 W was supplied to the electro-thermal source. It is evident when closely investigating the response of the sensor used for feedback control (T_{ETS}) that the location of this particular sensor is sub-optimal as the temperature settles very slowly at equilibrium in periods when the electro-thermal source is de-activated. It is also interesting to note that there is a negligible impact on temperature responses with respect to altitude variations. These are, as expected, a mere temperature bias and will, as such, not have any notable influence on the required temperature profiles.

Responses for the de-icing test flight were obtained at a an altitude of approximately 300 m, with an average airspeed of 17 m/s. The de-icing program routine was operated with a desired set point temperature of +20°C. Maximum available power was approximately 450W.

The responses displayed in Figure 7 obtained during the de-icing test flights show that the power supplied to the electro-thermal source is not adequate to reach the desired set point temperature. One of the strengths of the de-icing approach is a relatively low energy consumption, despite a higher requirement for immediate power. This strength is undermined by the lack of power and the duration of the activation sequence of the electro-thermal source (as exemplified by the responses in Figure 7), i.e. the 'on' period should be reduced and power increased for optimal de-icing functionality. Comparing the responses from all the electro-thermal source temperature sensors the pattern indicating a non-uniform temperature distribution in and over the electro-thermal source is maintained. Another thing to note is the initial responses (the initial spikes) of the T_{ets} group of sensors, when the electro-thermal source is activated. One explanation to this pattern deviating behaviour could be that this group of sensors are located on top of the surface of the electro-thermal source (i.e. they were fitted after the initial retro-fit), as opposed to the sensor used for feedback control, which is embedded in the electro-thermal source.

The anti-icing test flight responses were obtained under conditions similar to the ones described for the de-icing test flights, except for the desired set point temperature, which for the anti-icing test flight was set to +5°C. The initial power consumption needed to reach the desired set-point temperature was approximately 450W. Once the set-point was reached power consumption settled at approximately 210W. The anti-icing program routine was deliberately terminated after 300 seconds as a precaution to ensure that the limitations of the power source were not exceeded.

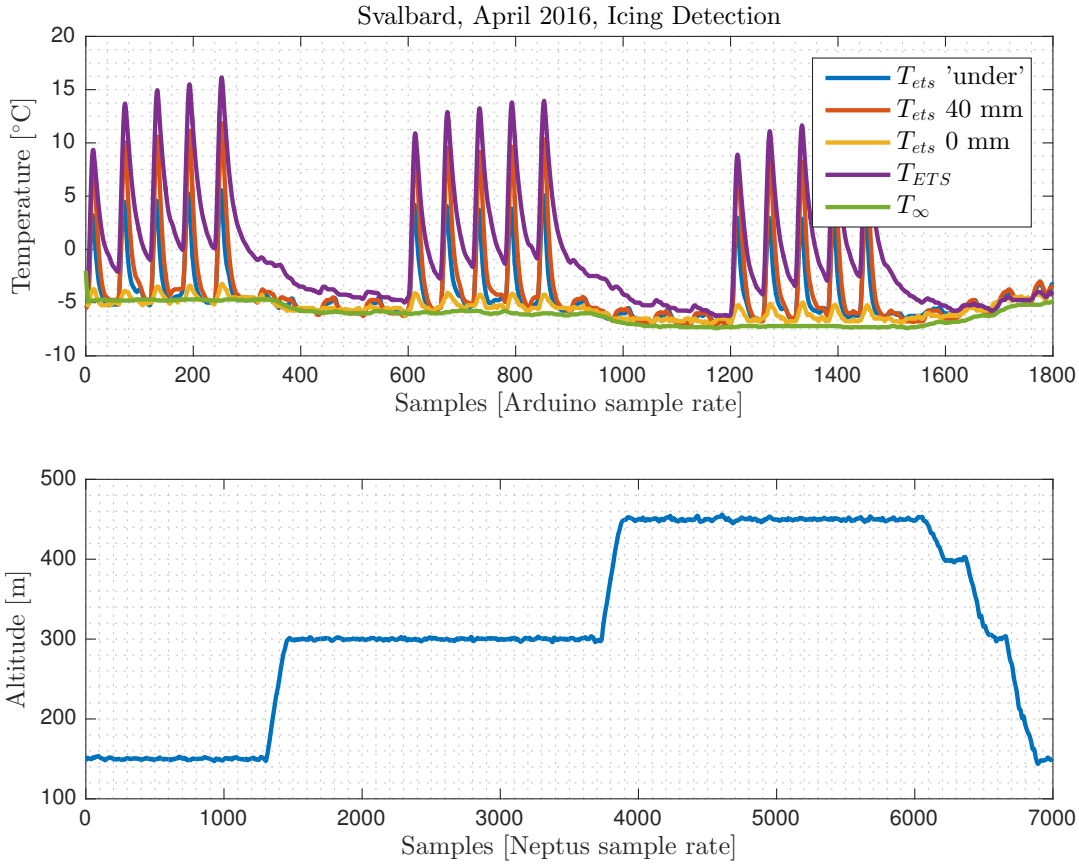

Fig. 6: Responses from the icing detection program routine test flights in Ny-Ålesund, Svalbard, in April 2016.

The temperature responses displayed in Figure 8 were obtained during the anti-icing test flight. The temperature sensor used for feedback control (T_{ETS}) clearly shows how the objective of maintaining the desired set point temperature is achieved, thereby demonstrating the feasibility of the anti-icing program routine. Investigating the responses of the sensor group denoted T_{ets}, the non-uniformity of the electro-thermal source temperature distribution once again becomes apparent. The relative periodic decreases/increases seen in the responses of the two T_{ets} sensors located 'atop' of the aerofoil can be attributed to a directional change of the aircraft.

IV. Conclusion

This paper is a presentation of a proof-of-concept study, of an autonomous icing protection solution for small unmanned aircraft, and includes findings from test flights conducted in Ny-Ålesund, Svalbard, Norway. All test flights were conducted in non-icing conditions.

Due to the integration of several extra temperature sensors strategically located around the leading edge of the wing, temperature responses were obtained that highlighted the non-uniformity of the thermal distribution over the electro-thermal sources. These results are as expected due to well known aerodynamic and thermodynamic phenomena. The responses also show that the control algorithms perform as required for each of the three categories of test flights (i.e. icing detection, anti-icing, and de-icing).

Finally, it is worth noting in the icing detection program routine test flight responses, is the little impact altitude variations have on the thermal time constant τ.

Acknowledgment

This work has been carried out at the Centre for Autonomous Marine Operations and Systems (NTNU-AMOS), supported by the Research Council of Norway through the Centres of Excellence funding scheme, Project number 223254. The Norwegian Research Council is acknowledged as the main sponsor of NTNU-AMOS.

Partial funding of the first experiments at Svalbard (2015): Autonomous Unmanned Aerial System as a Mobile Wireless Sensor Network for Environmental and Ice Monitoring in Arctic Marine Operations. Innovation project funded by the Research Council of Norway (235348) together with partners. Partial funding of the icing tunnel experiments: CIRFA – Centre for integrated remote sensing and forecasting for Arctic operations, funded by the Research Council of Norway (RCN project number 237906), together with the partners.

Gratitude needs to be expressed to Matthew Fladeland, programs manager at the airborne science program, at NASA-Ames Research Center, for sharing his expertise, assistance, and support during the completion of the research presented here.

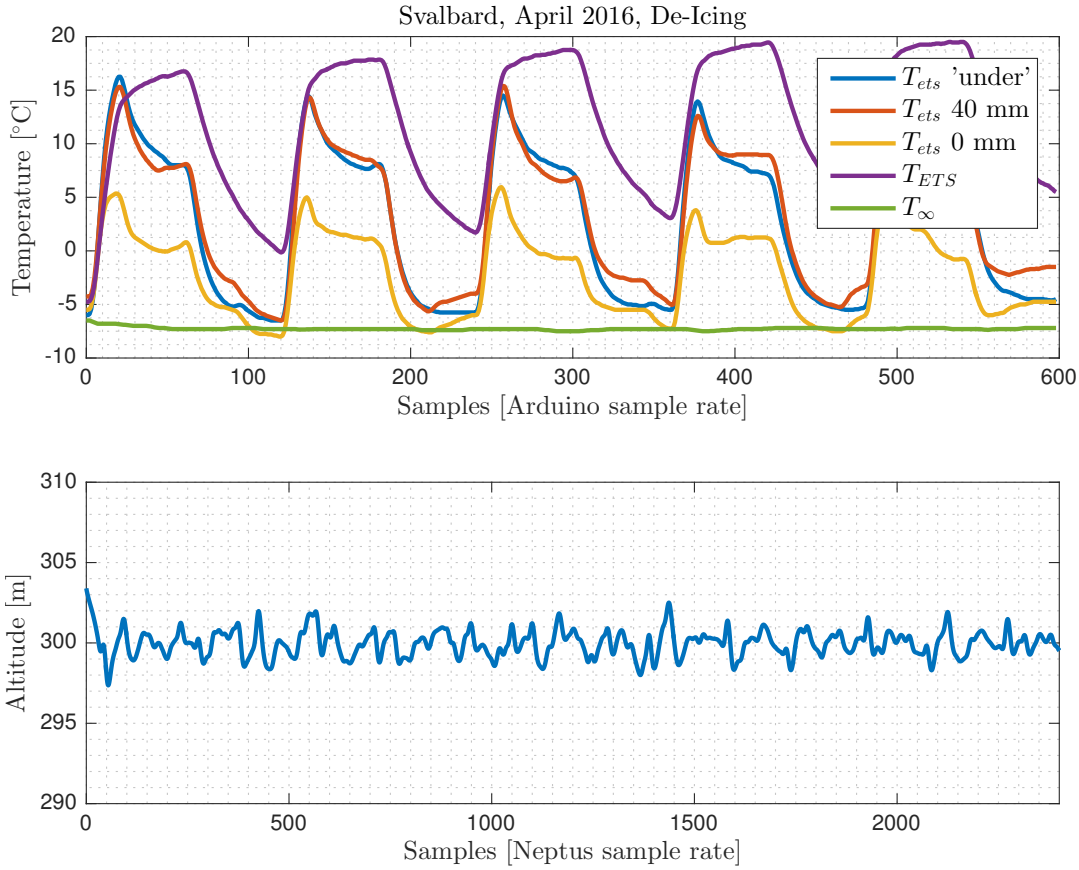

Fig. 7: Responses from the de-icing program routine test flights in Ny-Ålesund, Svalbard, in April 2016.

Gratitude should also be conveyed to the Northern Research Institute (NORUT), for their assistance and collaboration throughout the efforts presented in this paper.

Finally, deep gratitude should be expressed to the pilots of the NTNU-AMOS UAV research laboratory, for their diligence and patience, assistance and guidance.

References

[1] Research on inflight parameter identification and icing location detection of the aircraft. *Aerospace Science and Technology*, 29"(1):305 – 312, 2013.

[2] K.M. Al-Khalil and T.F.W. Ferguson. Hybrid ice protection system for use on roughness-sensitive airfoils, Mar 2001. US Patent 6,196,500.

[3] Fikret Caliskan and Chingiz Hajiyev. A review of in-flight detection and identification of aircraft icing and reconfigurable control. *Progress in Aerospace Sciences*, 60:12–34, 2013.

[4] A. Cristafaro, T. A. Johansen, and A. P. Aguiar. Icing detection and identification for unmanned aerial vehicles: Multiple model adaptive estimation. In *European Control Conference*, July 2015.

[5] A. Cristofaro and T. A. Johansen. An unknown input observer based control allocation scheme for icing diagnosis and accommodation in overactuated uavs. In *European Control Conference*, July 2016.

[6] Sergio Fernández-González, José Luis Sánchez, Estíbaliz Gascón, Laura López, Eduardo García-Ortega, and Andrés Merino. Weather features associated with aircraft icing conditions: A case study. *The Scientific World Journal*, page 18, 2014.

[7] Svein M Fikke, Jón Egill Kristjánsson, and Bjørn Egil Kringlebotn Nygaard. Modern meteorology and atmospheric icing. In *Atmospheric Icing of Power Networks*, pages 1–29. Springer, 2008.

[8] Omid Gohardani. Impact of erosion testing aspects on current and future flight conditions. *Progress in Aerospace Sciences*, 47(4):280 – 303, 2011.

[9] Seth S. Kessler, Christopher T. Dunn, Sunny S. Wicks, Roberto Guzman de Villoria, and Brian L. Wardle. Carbon nanotubes (cnt) enhancements for aerosurface state awareness. In *8th International Workshop on Structural Health Monitoring*, 2011.

[10] Alexei Korolev and George A. Isaac. Relative humidity in liquid, mixed-phase, and ice clouds. *Journal of the Atmospheric Sciences*, 63(11):2865–2880, 2006.

[11] Amanda Lampton and John Valasek. Prediction of icing effects on the coupled dynamic response of light airplanes. *Journal of Guidance, Control, and Dynamics*, 31(3):656–673, August 2008.

[12] By James P. Lewis and Dean T. Bowden. Preliminary investigation of cyclic de-icing of an airfoil using an external electric heater. Technical report, National Advisory Committee for Aeronautics. Ames Aeronautical

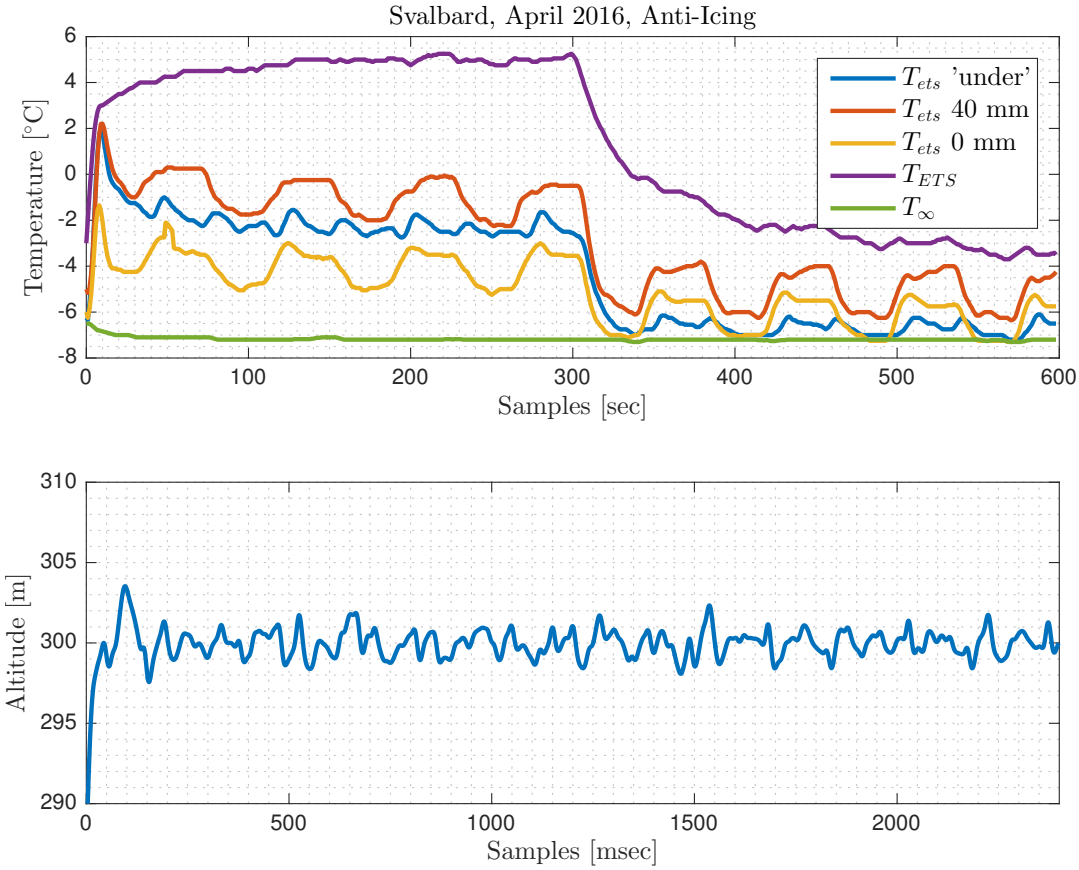

Fig. 8: Responses from the anti-icing program routine test flights in Ny-Ålesund, Svalbard, in April 2016.

Lab.; Moffett Field, CA, United States, February 1952.

[13] T. G. Myers. Extension to the messinger model for aircraft icing. *AIAA Journal*, 39(2):211–218, 2001.

[14] Mahdi Pourbagian and Wagdi G. Habashi. Aero-thermal optimization of in-flight electro-thermal ice protection systems in transient de-icing mode. *International Journal of Heat and Fluid Flow*, 54:167–182, 2015.

[15] Patrice Rauch and Jean-Cyril Bauchet. Resistive elements for heating an aerofoil, and device for heating an aerofoil incorporating such elements, Oct 1999. US Patent 5,971,323.

[16] D. Rotondo, A. Cristofaro, T. A. Johansen, F. Nejjari, and V. Puig. Icing detection in unmanned aerial vehicles with longitudinal motion using an lpv unknown input observer. In *2015 IEEE Conference on Control Applications (CCA)*, pages 984–989, Sept 2015.

[17] D. Rotondo, A. Cristofaro, T. A. Johansen, F. Nejjari, and V. Puig. Detection of icing and actuators faults in the longitudinal dynamics of small uavs using an lpv proportional integral unknown input observer. In *3rd International Conference on Control and Fault-Tolerant Systems*, Sept 2016.

[18] R.B. Rutherford and R.L. Dudman. Zoned aircraft de-icing system and method, may 2001. US Patent 6,237,874.

[19] Paul Schultz and Marcia K. Politovich. Toward the improvement of aircraft-icing forecasts for the continental united states. *Weather and Forecasting*, 7(3):491–500, 1992.

[20] K. L. Sorensen. *Autonomous Icing Protection Solution for Unmanned Aircraft*. PhD thesis, The Norwegian University of Science and Technology, 2016.

[21] K. L. Sørensen, M. Blanke, and T. A. Johansen. Diagnosis of wing icing through lift and drag coefficient change detection for small unmanned aircraft. *IFAC - PapersOnLine*, 48(21):541–546, 2015.

[22] K. L. Sørensen, A. S. Helland, and T. A. Johansen. Carbon nanomaterial-based wing temperature control system for in-flight anti-icing and de-icing of unmanned aerial vehicles. In *IEEE Aerospace Conference*, March 2015.

[23] Gregory Thompson, Roelof T. Bruintjes, Barbara G. Brown, and Frank Hage. Intercomparison of in-flight icing algorithms. part i: Wisp94 real-time icing prediction and evaluation program. *Weather and Forecasting*, 12(4):878–889, 1997.

[24] M.M. Tousi and K. Khorasani. Fault diagnosis and recovery from structural failures (icing) in unmanned aerial vehicles. In *3rd Annual IEEE Systems Conference*, pages 302–307, March 2009.

[25] M.M. Tousi and K. Khorasani. Robust observer-based fault diagnosis for an unmanned aerial vehicle. In *IEEE International Systems Conference (SysCon)*, pages 428–434, April 2011.